Crystalline Structure and Properties of EP and EB Copolymers by Solid-State NMR, DSC, and WAXS

Weiguo Hu,*,† Srivatsan Srinivas,† and Eric B. Sirota‡

ExxonMobil Chemical Company, 5200 Bayway Drive, Baytown, Texas 77520-2101, and ExxonMobil Research and Engineering Company, 1545 Route 22 East, Annandale, New Jersey 08801-0998

Received October 26, 2001; Revised Manuscript Received March 30, 2002

ABSTRACT: The crystalline structures of ethylene−propylene (EP) and ethylene−butene (EB) copolymers have been investigated using a combination of solid-state NMR, WAXS, and DSC. In high-propylene (>20 mol %) EP copolymers, the α methylene exhibits different isotropic chemical shifts in the crystalline and amorphous regions. This indicates the presence of the methyl branch in the crystalline region and that the branch point has a trans conformation. As a result of the incorporation, on increasing branch content, the orthorhombic lattice expands in the EP copolymers. Then they exhibit a first-order transition from orthorhombic to a rotator (hexagonal) phase in which chains rotate about the chain axes. In the rotator crystals, about 5% of the carbons are methyl groups. At lower propylene comonomer contents, the crystal structure is orthorhombic, although with a larger area per chain and lower-field isotropic chemical shift value than observed for HDPE. It is proposed that the pattern of change of lattice constants and eventual transition into the rotator phase upon increasing branch content are closely related to the dynamics of the crystalline chains. In EB copolymers, in contrast, even at high comonomer concentrations, the crystal structure is still orthorhombic. The measured expansion coefficient of the rotator phase is much less than that of the same phase in *n*-alkanes, likely due to temperature-dependent branch incorporation.

Introduction

It has been speculated that the difference in physical properties between ethylene−propylene (EP) and ethylene−butene (EB), ethylene−hexene (EH), and ethylene−octene (EO) polymers is due to incorporation of the methyl branch in the polyethylene crystal and the exclusion of ethyl and longer branches from the polyethylene crystal, due to their larger sizes. A variety of wide-angle X-ray (WAXS) studies have shown that propylene units are incorporated in the orthorhombic polyethylene crystal in EP copolymers.[1−6] This incorporation is manifested as an increase in the *a*-axis of the orthorhombic unit cell with increasing propylene content.[1,3] When the *a*-axis equals $b\sqrt{3}$, the unit cell is hexagonal. Similar to orthorhombic crystallites in low-density ethylene copolymers, the crystallization of the hexagonal phase is also very slow.[7] There are fewer studies dealing with the existence of the hexagonal form in ethylene copolymers with higher α-olefins, although Androsch et al. have reported[8] that ethylene−octene copolymers with high comonomer content show coexistence of the orthorhombic, hexagonal, and amorphous phases. The hexagonal phase content was also found to increase on drawing the sample.[1,5] The explanation offered in the literature as to the presence of the hexagonal phase at room temperature and atmospheric pressure was that defects in the form of side groups stabilized the hexagonal phase at room temperature.

The hexagonal phase in homo-polyethylene is not thermodynamically stable at atmospheric pressure; however, it occurs between the orthorhombic crystal and the melt at high pressures. This hexagonal phase is similar in many respects to the hexagonal rotator phase observed in shorter *n*-alkanes. In linear polyethylene under high pressure, the hexagonal phase is characterized by a high degree of conformational disorder. In alkanes, the rotator phase's symmetry is defined by the lack of long-range rotational order of molecules about their long axis. For short alkanes, even in the absence of dominating conformational disorder, the rotator phase exists since the short molecules can rotate independently of each other (even though rotator phases do contain some chain-end conformational disorder). The rotator phase has been studied in great detail in these short alkanes.[9] In extended chain crystals of polymers (or longer alkanes) the rotation of the plane associated with the carbon−carbon bonds is more likely to be associated with conformational disorder. Thus, the hexagonal phase in high pressure (unbranched) polyethylene is one with an entropy closer to that of the melt compared to the rotator phase in shorter alkanes.[10] This is in line with the study of constrained ultradrawn polyethylene fibers using solid-state NMR which suggests that the hexagonal phase contains a considerable number of gauche defects.[11]

In short *n*-alkanes, the rotator phase has been shown to mediate nucleation of crystallization,[12] and a metastable form of the hexagonal phase has been suggested as being important in the nucleation of polyethylene.[13,14] The understanding of the stability mechanisms of such weakly ordered phases may yield new insights into the mechanisms of polymer crystallization.

For EP copolymers, when the propylene content is high (>20 mol %), only one major crystalline WAXS reflection is present. This makes it difficult to unambiguously determine the crystalline structure. Using solid-state NMR which is capable of investigating the crystalline form and chemical structure simultaneously, one could investigate the inclusion of side groups in the crystallites as well as determine the mode of motion of

† ExxonMobil Chemical Company.
‡ ExxonMobil Research and Engineering Company.
* Corresponding author: Fax (281)834-1793; e-mail weiguo.hu@exxonmobil.com.

10.1021/ma0118670 CCC: $22.00
Published on Web 05/21/2002

Table 1. Molecular Weights and Comonomer Contents of Ethylene Copolymers Used in Current Study

		comonomer content				
sample	comonomer	mol %	wt %	ϕ	M_w	M_w/M_n
EB0	butene	~0	~0	~0		
EB8	butene	7.8	14.5	0.039		
EB11	butene	11.4	20.5	0.057	118K	2.1
EB16	butene	15.6	27.0	0.078	59K	2.1
EP8	propylene	7.9	13.5	0.0471	75K	2.2
EP10	propylene	10.1	15.3	0.0537	285K	3.0
EP13	propylene	12.8	18.1	0.0642		
EP19	propylene	19.3	26.4	0.0965		
EP20-1	propylene	19.9	27.2	0.0997		
EP20-2	propylene	20.4	27.8	0.1021		
EP20-3	propylene	19.8	27.0	0.099	74K	2.1
EP22	propylene	22.4	30.2	0.1119		
EP27	propylene	26.7	35.3	0.1334		

the crystalline chains. Evidence from solid-state NMR[15] and fuming nitric acid treatment[16] studies showed that propylene units (methyl side groups) can be incorporated into the orthorhombic crystal. Ethyl branches were also found to exist in the crystalline regions, however at a much lower concentration.[16,17] In these studies, only polymers with very low comonomer concentrations (<5 mol %) were studied.

The objective of this study is to investigate the structure and properties of ethylene copolymers with propylene and butene at larger comonomer contents. Experimental results from solid-state NMR, WAXS, DSC, and mechanical measurements are discussed in order to understand the nature of the crystalline phase (orthorhombic vs hexagonal, rotation vs flip, side branch incorporation vs exclusion) and its effect on the structure and properties of the polymers.

Experimental Section

The copolymer samples used in this study were all synthesized using single-site metallocene catalysts. Polymers made with such catalysts are typically characterized by narrow molecular weight distribution and narrow composition distribution. All samples were molded between the platens of a hot press at 180 °C. The samples were then quenched between the chill platens of the hot press. The samples were stored at room temperature for at least a month prior to any tests being conducted. The ethylene contents of the polymers were determined using solution ^{1}H NMR. The molecular weights of the samples were determined from GPC measurements. No corrections to the GPC data were made for the different comonomer type and comonomer contents. The characteristics of the samples used are shown in Table 1. For convenience, the nomenclature of the sample ID was chosen such that the first part of the name contains the copolymer type and second part contains the comonomer mole percentage. An additional number is assigned to each sample where several samples have the same mole percentage. ϕ is defined as the fraction of backbone carbons containing a methyl branch (or an ethyl branch for the case of the ethylene−butene copolymers); i.e., ϕ and mole content are different by a factor of 2.

Four solid-state NMR techniques were utilized to obtain a comprehensive understanding of the materials: (1) ^{1}H to ^{13}C cross-polarization/magic-angle spinning experiment (CP/MAS). This technique suppresses signals from the mobile component (amorphous phase) so that even a small fraction of the crystalline component shows up prominently in the spectrum. Contact times were 0.06−1 ms. (2) ^{13}C direct polarization/magic-angle spinning experiment (DP/MAS) which allows quantitative measurement of comonomer content and crystallinity. Recycle delay was 20−500 s depending on the crystalline ^{13}C T_1 relaxation time of the samples. (3) CP/^{13}C T_1 filter experiment[18] which was used to (a) measure ^{13}C T_1 relaxation time or (b) fully remove the mobile component from the spectrum. A T_1 filtering time of 0.5−500 s was used to partially or fully relax the amorphous signals. (4) CP/^{1}H $T_{1\rho}$ filter experiment. 2−10 ms of filtering time was used to relax the amorphous signals in order to determine the branch concentration in the crystalline phase. All the experiments were performed on a Bruker DSX-500 spectrometer, with a ^{1}H frequency of 500.13 MHz and ^{13}C frequency of 125.75 MHz. The sample spinning speed in all the MAS experiments was 4 kHz. The decoupling power was 80 kHz. A ^{1}H 90° pulse length was 4 μs. All the spectra were calibrated with reference to the crystalline signal in high-density polyethylene, which is set at 32.8 ppm.

X-ray scattering measurements were performed using a Rigaku 18 kW rotating anode X-ray generator with a copper anode. Cu Kα radiation was selected using a vertically bent graphite monochromator which also focused the beam. The beam size at the sample was determined by slits to be 1 mm horizontal and 2 mm vertical. The sample was located in the center of a Huber two-circle diffractometer. The scattering beam was detected using a Bicron single channel detector behind a horizontal 1 mm wide slit. This gave an arm-zero full width half-maximum of ~0.12°.

The samples were contained in a temperature-controlled oven that was made of copper and contained Kapton windows through which the X-rays could pass. The oven was cooled with ethylene glycol from a chiller, and the temperature was controlled dynamically using thermoelectric heating/cooling elements.

The entire experiment was automated using Spec software from Certified Scientific running on a LINUX operating system and interfaced using CAMAC hardware.

Some initial measurements were performed at ExxonMobil's beamline X10A at the National Synchrotron Light Source at Brookhaven National Laboratory. These measurements showed that there were no sharp features at high angles for which the high resolution available at the synchrotron was necessary. The detailed temperature-dependent measurements were then carried out on the rotating anode source.

A large suite of samples were studied with X-rays, as also shown in Table 1. All samples had been annealed at room temperature for at least 1 month before performing the X-ray scans. The samples were then cooled below room temperature and heated above room temperature to obtain the thermal dependence of the lattice parameters.

The three possible phases of interest here are (a) the amorphous phase, characterized in wide-angle scattering by a broad peak at $q \sim 1.35$ Å^{-1}, (b) the orthorhombic herringbone crystal phase, characterized by sharp peaks at $q \sim 1.52$ and 1.68 Å^{-1}, and (c) the hexagonal phase, characterized by a single sharp peak at $q \sim 1.5$ Å^{-1}.

The X-ray scattering data were modeled using a form which included Lorentzian line shapes $I \propto 1/(1 + (q - q_p)^2\xi^2)$ for the two crystalline peaks and a Lorentzian plus a quadratic form for the amorphous scattering.[19] The data were fit using the CPLOT nonlinear least-squares fitting routine over the range 0.9 Å^{-1} < q < 1.9 Å^{-1}. The crystallinity was approximated by integrating the respective peaks between $q = 0.9$ and 1.9 Å^{-1}. While this method does not give an absolute crystallinity, it is sufficient for determining relative crystallinity values.

DSC experiments were carried out on ~12 mg of sample using a TA DSC 2910 at heating and cooling rates of 10 °C/min. The DSC was calibrated for temperature and heat flow using indium. The temperature at the peak of the endotherm was taken as the melting temperature, and the area under the peak was taken as the heat of fusion.

Mechanical measurements were performed on dogbone-shaped samples cut out of compression-molded films, using an INSTRON 4502 at crosshead speeds of 0.847 mm/s. At least five specimens were tested for each sample, and the average results are reported. The stress results were not corrected for changing cross section; i.e., the reported values are engineering stress. Permanent set measurements were carried out by stretching the sample to 200% of the original length (not including the original length) and immediately returning to

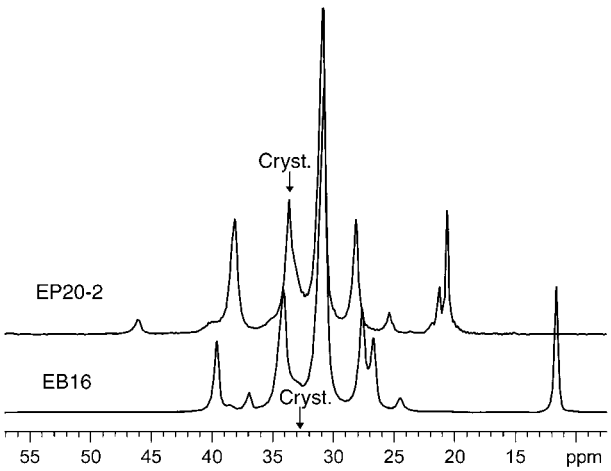

Figure 1. Fully relaxed DP spectra for EP and EB copolymers with similar comonomer concentration (16 and 20 mol %). The positions of the crystalline signals are indicated by the arrows. The EP copolymer has a prominent crystalline peak (crystallinity ~10%), while the EB copolymer has no discernible crystalline peak at the position indicated (crystallinity ≤2%).

the original state. The change in length relative to the original length was taken as the permanent set.

Results

Crystallinity and Comonomer Concentration Measurement. The crystallinity of EP copolymers was measured using a solid-state NMR method originally developed for measuring crystallinity in high-crystallinity polyethylene.[20] Basically, the crystallinity is determined from the area ratio of crystalline and amorphous signals in the direct-polarization (Bloch decay) spectrum. The crystalline signal was corrected for incomplete relaxation, the extent of which is determined by the CP/^{13}C T_1 experiment. In the case of EP copolymers, additional complexity is introduced by the fact that the methine signal merges with the crystalline peak at ~33 ppm. Therefore, the crystalline signal is determined by subtracting the methine signal, which is known from the methyl signal area appearing at 20 ppm, from the area of the 33 ppm crystalline peak. Spinning sidebands were not integrated, which introduces about 5% relative error in the crystallinity data.

In the NMR spectra, the crystalline and amorphous CH_2 peaks are partially overlapping. In such cases, the integration was separated at the valley rather than going through curve deconvolution. The error in determination of crystallinity using this method can be estimated as within 2 percentage points. Various sources such as noise, signal in spinning sidebands, phase correction, and signal overlap are the major contributors to errors.

Figure 1 shows the NMR spectra of an EP and an EB copolymer. Major peaks arising from comonomer structures appear very close to their respective positions in solution NMR spectra and have been well assigned. The crystalline signal at ~33 ppm is marked in the figure. As seen in the figure, the crystallinity of EB16 is so low that the crystalline signal does not appear as a distinct peak. Therefore, the crystallinity cannot be determined for this sample using this method (estimated as 2%, see Figure 8f). The crystallinities of some of the other samples have been estimated and are shown in Table 2. Note that, as expected, the crystallinity decreases with increasing comonomer content. An interesting observation is that the EP copolymer with a higher fraction of comonomer (EP20-2) has a substantially higher degree of crystallinity than the EB copolymer with a lower comonomer content (EB16). This indicates that ethyl branches are more effective in disrupting crystallinity than methyl branches. The WAXS and DSC data discussed later show identical trends with respect to increasing propylene content and the difference between propylene and butene comonomers.

Table 2. Crystallinity, Comonomer Content, and Branch Concentration in the Crystalline Phase Determined by Solid-State NMR

sample ID	comonomer mol % SSNMR	comonomer mol % soln ^{1}H NMR	crystallinity (%)	branch concn in crystal (per 100 carbon)	partitioning factor (*c*:*a*)
EP8	6.9	7.9	53		
EP10	10.7	10.1	34	2	1:3.5
EP13		12.8		2.7	1:2.4
EP20-2	19.0	19.8	13	5	1:2
EB16	16.0	15.6	2		

As will be discussed in detail later, we believe this is because the methyl units are incorporated in the crystal, whereas the ethyl units are predominantly excluded from the crystal. A consequence of this exclusion is that the fraction of continuous ethylene sequences that can crystallize decreases with increasing butene content, leading to lower crystallinity. However, since methyl units can be incorporated in the crystal, increasing propylene content does not cause as large a decrease in crystallinity. This is also supported by WAXS data (discussed later) that show the incorporation of propylene units in the crystals to be greater than the incorporation of butene units.

The comonomer weight concentration of the EP copolymers can be estimated as the total area of the methyl signal plus $S_{\alpha\delta+}$ (methylene next to a methine group) divided by the total signal area. The comonomer weight concentration of the EB copolymers can be estimated as the total area of the methyl signal plus the signal between 26 and 29 ppm divided by the total signal area. The comonomer concentrations determined this way are shown in Table 2. A comparison between the comonomer contents calculated using this method with the values determined using solution ^{1}H NMR shown in Table 1 indicates good agreement between the two methods.

Evidence of "Rotator" Phase in EP Copolymers. CP/MAS spectra of a series of EP copolymers and a polyethylene homopolymer (a gel-spun ultrahigh molecular weight polyethylene fiber, Spectra900) are shown in Figure 2. Short CP times (60−100 μs) were chosen so that the crystalline signal is more prominent in the spectrum. The isotropic chemical shift (ICS) of the crystalline peak shifts downfield from 32.8 to 33.4 ppm as the propylene content increases and stays at 33.4 ppm for propylene contents ≥20 mol %. The crystalline peaks in EP20-2 and EP27 appear at 33.4 ppm, which coincide with that often observed for the rotator phase in *n*-alkanes. For example, Ishikawa et al. observed that the rotator phases of *n*-$C_{19}H_{40}$, $C_{24}H_{50}$, and $C_{32}H_{66}$ have a chemical shift of 33.4 ppm.[21] These three materials at the temperatures studied exhibit three different rotator phases: the R_I (an untilted orthorhombic structure), the R_{II} (hexagonal), and R_{III} (nearly hexagonal and tilted);[22] however, the chemical shifts for all were essentially the same. A similar signature of the rotator

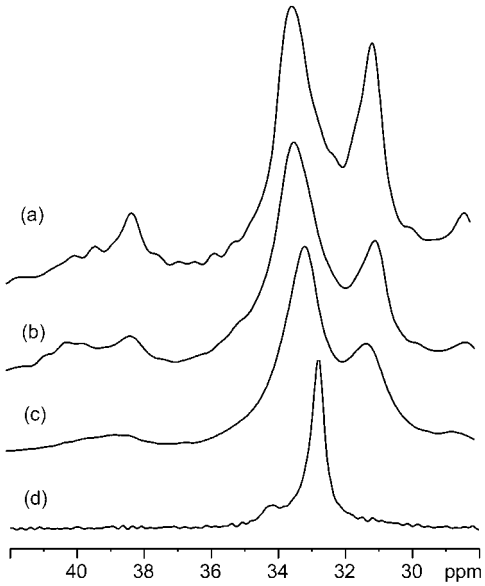

Figure 2. CP/MAS spectra of (a) EP27, (b) EP20-2, (3) EP13, and (d) linear PE. Note the shift of the crystalline peak as a function of methyl branch content.

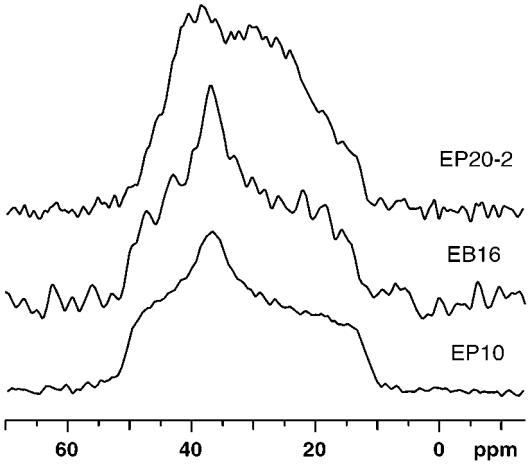

Figure 3. Crystalline phase nonspinning spectra of EP and EB copolymers. In EP10 and EB16, the line shape exhibits characteristics of a static phase. For high-propylene EP (EP20-2), the spectrum is typical of a rotator phase.

phase has also been observed in *n*-octadecanol.[23] The reason why the ICS's of orthorhombic, rotator, and monoclinic phases are different has not been fully understood;[24] a tentative explanation is given in the "Discussion" section. In the rotator phase, the crystalline stems rapidly rotate about the chain axis, without destroying the in plane order; i.e., positional correlations perpendicular to the chain axis are maintained.

The rapid rotation of the crystalline stems in the crystal can be conveniently examined using the powder pattern, i.e., a nonspinning spectrum of an isotropic sample. The powder patterns of EP and EB copolymers are shown in Figure 3. For EP10 and EB16, a short CP time and ^{13}C T_1 filter were applied to suppress the amorphous signal to the largest degree. Their line shapes exhibit characteristics of a static unit: two shoulders and one tip indicate a chemical shift tensor with three different principal values. A 180° flip motion of the polyethylene chain[25−27] would leave the chemical shift principal values unchanged, which would also result in the same pattern. EP13 also exhibits a similar powder pattern (not shown), indicating its crystallites are orthorhombic even though its ICS is shifted to 33.1 ppm. On the other hand, for the high propylene copolymer EP20-2, the spectrum exhibits only two principal values: one tip on the left and one shoulder on the right. This is because the two chemical shift principal values whose axes are perpendicular to the chain axis are averaged due to rapid chain rotation. Therefore, this is further evidence of a rotator phase in high propylene EP copolymers. Because the crystalline $T_{1,C}$ is quite short (discussed later) for EP20-2 due to the high mobility of the crystalline stems, a $T_{1,C}$ filter would not be effective in suppressing the amorphous signal. Although a short CP time (60 μs) was used to suppress the amorphous signal as much as possible, the suppression is not complete, and some residual broad amorphous signal can be found in the vicinity of 30 ppm.

It is interesting to note that, even though the crystallinity of the EB copolymer is much smaller than the EP copolymer, the crystalline stems in the EB copolymer are not rotating, which indicates a fundamental difference between the nature of the crystallites in these copolymers. The motion in the crystallites in the EB copolymers corresponds to 180° flip, as is observed in linear PE or EP copolymers with low propylene content.

It can be noticed in Figure 3 that the left edge of the powder pattern at ∼45 ppm of EP20-2 is not as steep as that observed for a small molecule rotator phase (for example, 1,22-docosanediol[28]), even though it is sufficiently different from that of EB16. This corroborates with what was observed in Figure 2, where the crystalline peak in the EP copolymer is much broader than that of HDPE, which could be due to a combination of several mechanisms: the Rothwell−Waugh effect, motion being partially disordered,[5] existence of varied levels of motional freedom, a distribution of chemical shift, etc. This suggests that the rotator phase in EP copolymers contains much more disorder than that in *n*-alkanes and their derivatives. This is possibly because the former is looser-packed, which gives the ethylene segments more space to move. On the other hand, the area per chain of the rotator phase (21 Å^2) is not big enough for a rotation that is totally free of disturbing neighboring chains; such a phase would require an area of ∼25 Å^2 per chain. Nevertheless, based on the isotropic chemical shift (ICS), EP copolymers display a much better defined rotator phase than the hexagonal phase in constrained ultradrawn PE fibers, which contains a substantial amount of gauche conformations and exhibit an ICS which is shifted upfield relative to the orthorhombic signal.[11]

Quantification of Methyl Branch Concentration in Crystallites. To assign signals associated with crystalline regions, spectra of EP20-2 in the semicrystalline state (ambient temperature) and molten state (50 °C) were acquired for comparison (see Figure 4). A comparison of the two spectra indicates that the semicrystalline spectrum has two additional peaks at 33.4 and 40 ppm. The 33.4 ppm peak is from crystalline main chain methylene, while the 40 ppm peak can be assigned to the crystalline methylenes that are next to a methine group (referred to as $S_{\alpha\delta+}$,[29] or α carbon). Their corresponding amorphous signals are at 31 and 38 ppm, respectively. The splitting of the $S_{\alpha\delta+}$ signal is about 1.7 ppm. The different chemical shifts that $S_{\alpha\delta+}$ exhibits in crystalline and amorphous environments are due to different conformation: crystalline segments maintain an all-trans conformation, while amorphous segments

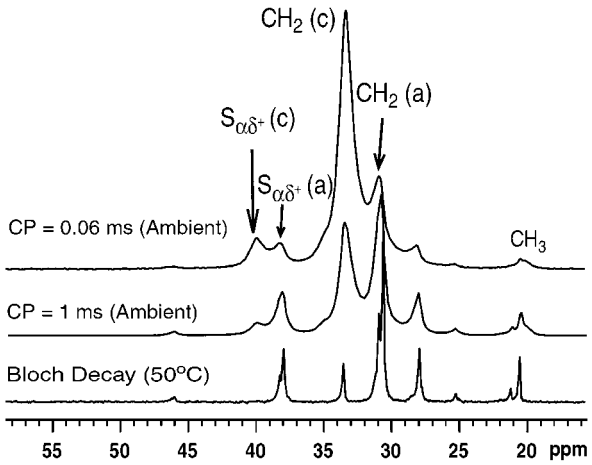

Figure 4. CP and Bloch decay spectra of EP20-2. Identification of crystalline signals can be made through comparison of molten and semicrystalline states as well as different contact times that result in different crystalline/amorphous weightings.

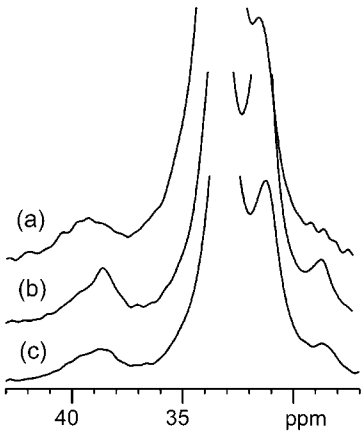

Figure 5. Spectra of EP13 with different crystalline/amorphous signal ratio weightings, indicating the position and shape of $S_{\alpha\delta+}$ resonance in crystalline and amorphous regions: (a) CP/$T_{1,C}$ filtered spectrum with contact time = 80 μs, filter length = 0.5 s; (b) CP spectrum with contact time = 1 ms; (c) CP spectrum with contact time = 80 μs. The $S_{\alpha\delta+}$ resonance is mostly crystalline in (a) and has various amount of amorphous content in (b) and (c).

experience a dynamical average of various conformational states.

A second method to identify the signal associated with crystalline regions is to vary the cross-polarization (CP) time. Rigid segments have much larger CP efficiency than mobile segments; therefore, the signal from rigid segments increases quickly with CP time, while the signal from mobile segments needs much longer CP time to show up in the spectrum. In Figure 4, the spectra of EP20-2 having different amorphous/crystalline weighting by varying the CP time clearly show that the signals at 33.4 and 40 ppm are enhanced significantly at short CP times (which relatively enhances the rigid component). Therefore, these two peaks can be assigned to the crystalline regions. A similar amount of splitting was also observed for EP27 (not shown here).

Under the reasonable assumption that the CP efficiencies for crystalline $S_{\alpha\delta+}$ and main-chain methylene are the same, the concentration of methyl group in the crystalline phase can be calculated as half the area ratio of 40 and 33.4 ppm peak. For EP20-2, about 5% of the carbons in the crystalline region are from methyl groups. Knowing the overall composition and the crystallinity, the partitioning coefficient can be calculated to be $\sim^1/_2$, which means that in EP20-2 the methyl branch concentration in crystallites is about $^1/_2$ that in amorphous region. Note that this value is larger than reported in the literature for EP copolymers having smaller overall propylene contents.[15,16] Approximately the same methyl concentration in crystallites (~5%) was obtained for EP27, which possibly suggests that the rotator phase has a relatively constant methyl branch concentration, independent of the overall methyl branch content. This may be correlated with the observations that the lattice constants for the rotator phase do not change with composition (Figure 8a) and that the crystalline methyl concentration has a monotonic relationship with lattice constants.

There is less splitting between the $S_{\alpha\delta+}$ signals in the orthorhombic and the amorphous phases, as observed in Figure 5, as also reported in the literature.[15] For EP13 that has quite a large propylene content and expanded lattice, the splitting is about 0.7 ppm, which is much smaller than that observed for EP20-2. The crystalline $S_{\alpha\delta+}$ signal appears at 39.2 ppm, as compared with 40.0 ppm for the rotator phase. It is also broader, with a full width at half-maximum of ~2 ppm, in contrast to ~1 ppm for $S_{\alpha\delta+}$ in the rotator phase, indicating a larger dispersion of conformation or strain. The narrow signal width and the significant splitting of the $S_{\alpha\delta+}$ peak in the rotator phase suggest that the segments adjacent to a branching point have a trans conformation, while those in the orthorhombic phase slightly deviate from the trans conformation. Such a difference may be interpreted in terms of different modes of motion: continuous rotation of a chain in a crystalline environment is more effective in straightening the branching point than does flip motion, which is discontinuous.

Because of the lack of distinguishable splitting, determination of the methyl branch concentration in the orthorhombic phase is more difficult. VanderHart and co-workers[15,17] used $T_{1\rho}$ filter to obtain the weight of crystalline and amorphous contributions in the overlapping signal. An alternative method would be using ^{13}C T_1 filter experiment. The ^{13}C T_1 filter method assumes that the crystalline $S_{\alpha\delta+}$ has a much longer ^{13}C T_1 than the amorphous $S_{\alpha\delta+}$, while the ^1H $T_{1\rho}$ method assumes that the crystalline and amorphous $S_{\alpha\delta+}$ have the same ^1H $T_{1\rho}$'s as their respective neighboring CH_2 units. The former assumption requires the dynamics of $S_{\alpha\delta+}$ to be similar to a main-chain methylene and the relaxation driven by methyl rotation to be small. We found that using the ^{13}C T_1 filter method, when the filter length is sufficiently long (~10 s), a spectrum free of amorphous signal can be obtained, so no spectrum editing is necessary to obtain the crystalline methyl concentration (i.e., population ratio of methyl vs total carbon in the crystalline region), which is simply half the ratio of $S_{\alpha\delta+}$ and main CH_2 peak area. The methyl branch concentration and partitioning factor determined this way are listed in Table 2 (except for EP20-2 results, which were calculated using a different technique; see previous section). However, this method may underestimate the branch concentration in crystallites since the ^{13}C T_1 of $S_{\alpha\delta+}$ has an additional contribution from neighboring methyl rotation. On the other hand, the $T_{1\rho}$ filter method usually does not completely filter out the amorphous signal, and spectrum editing is needed to

Table 3. Magnetic Relaxation Times for Several EP and EB Copolymers

sample ID	comonomer mol %	crystallinity (%)	T_m (°C)	$T_{1,C}$(c) (s)	$T_{1,C}$(a) (s)	$T_{1\rho}$(c) (ms)	$T_{1\rho}$(a) (ms)
EP8	6.9	53	101.0	100			
EP10	10.7	34	82.1	41		2.6	3.5
EP20-2	19.0	13.6	45.3	1.1	0.7		
EB16	16.0	<2	46.2	10.5		2.1	3.0

calculate the crystalline branch concentration. We found that the crystalline branch concentration determined using the ^{13}C T_1 method usually yields a smaller result than the $T_{1\rho}$ method (simple integration; no spectrum editing performed), but the difference is within a factor of 2.

Magnetic Relaxation Times. Magnetic relaxation times of several EP and EB samples were measured as an additional approach to probe the molecular dynamics in the crystallites (Table 3). As seen from the table, in the series of EP copolymers, the crystalline ^{13}C T_1 decreases with increasing propylene content, which is consistent with the well-known observation that thinner crystallites result in shorter ^{13}C T_1 relaxation times[30] (due to faster chain diffusion). The crystalline phase in EP20-2 has a very short ^{13}C T_1 (1.1 s). This may be compared with the ^{13}C T_1 in the rotator phase of *n*-alkanes and derivatives, which is ~5 s.[23] Such a short relaxation time is unlikely the result of flip motion occurring in thin orthorhombic crystallites, since flip motion results in only indirectly bonded $^{13}C-^{1}H$ dipolar coupling fluctuations that drive the relaxation. For example, the ^{13}C T_1 of EB16 is considerably longer than that for EP20-2. On the other hand, continuous rotation will cause fluctuation of dipolar coupling between directly bonded ^{13}C and ^{1}H, which can result in a very short ^{13}C T_1 relaxation time. This is consistent with the earlier observations that the chains in EB crystals are flipping, and the chains in hexagonal EP crystals are rotating. From the ^{13}C T_1 value and a correlation between $T_{1\rho}$ and flip rate,[27] it can be roughly estimated that the flip rate in EB16 crystallites is $>10^4$/s. Therefore, the crystalline chains in orthorhombic EB16 also exhibit fast dynamics.

Wide-Angle X-ray Results. In Figure 6a–d we show typical X-ray scans of several EP copolymers at various temperatures (see caption) along with the fitted functional forms. In addition, the individual peak components of the fitted forms are also plotted. These four scans show a variation with ϕ in the relative strength of the second crystalline peak. In Figure 6a,b the second peak is clearly observable by eye. In Figure 6c the second peak is only apparent by eye as a hump on the first peak; however, the fitting identifies a well-defined peak as shown in the figure. For Figure 6d a second crystalline peak cannot be identified even by fitting, and the data are well represented by an amorphous phase and a single crystalline peak. The data for all the samples and temperatures were similar to these and fit accordingly.

As we will discuss in detail below, our overall data indicate a variation from an orthorhombic to a hexagonal crystal on increasing comonomer content, as also shown by SSNMR. Note that, since the primary reflection from the hexagonal phase appears at the same q value as the first peak of the orthorhombic phase, we cannot unambiguously determine the relative amounts of the orthorhombic and hexagonal forms that coexist

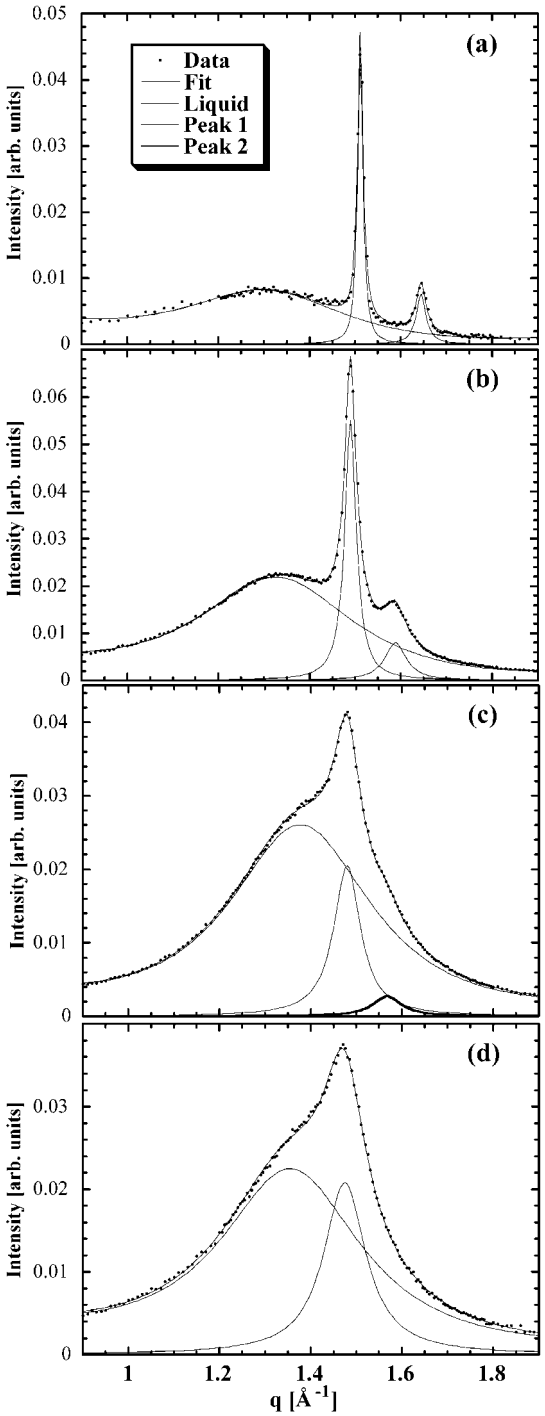

Figure 6. q-scans along with fits for EP copolymers (a) $\phi = 0$, $T = 78$ °C; (b) $\phi = 0.0642$ (EP13), $T = 56$ °C; (c) $\phi = 0.1021$ (EP20-2), $T = -18$ °C; and (d) $\phi = 0.0997$ (EP20-1), $T = -15$ °C.

at higher comonomer contents. Although, when the higher q peak of the orthorhombic form vanishes, we can state that the sample is entirely in the hexagonal form.

The structure of each sample was measured over a range of temperatures. In Figure 7a, we show the temperature dependence of the crystalline peak positions (q_1 and q_2) for the $\phi = 0.0642$ sample (EP13). In Figure 7b we show the temperature dependence of the area/chain and crystallinity. In Figure 7c we show the area/chain and crystallinity as a function of temperature for the $\phi = 0.0997$ sample (EP20-1), which is in the

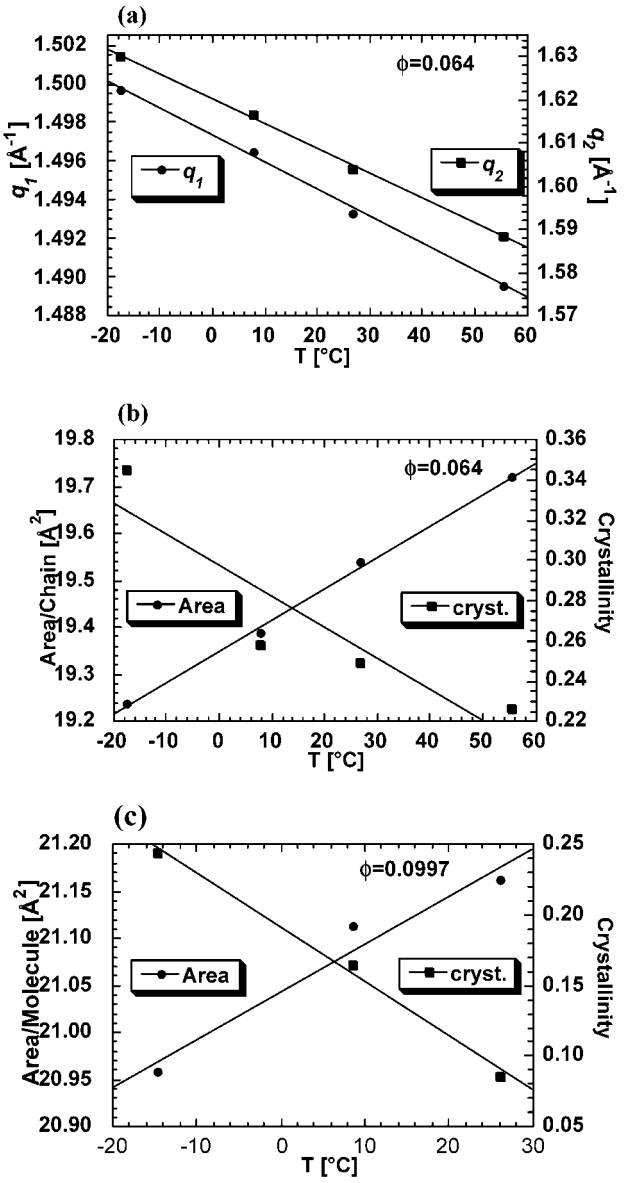

Figure 7. (a) Peak positions of the two orthorhombic peaks and (b) the crystallinity and the area/chain as a function of temperature for the $\phi = 0.064$ sample (EP13). (c) The crystallinity and area/chain for the $\phi = 0.0997$ sample (EP20-1). The lines are linear fits.

hexagonal phase. These show both thermal expansion and a significant falloff of crystallinity with increasing temperature. The increase in the degree of crystallinity with decreasing temperature is expected since segments with higher methyl branch concentrations and shorter ethylene sequences would be able to crystallize at lower temperatures. In such a case, one might expect that this would increase the incorporation of propylene units in the crystalline phase. If this were indeed to happen, one would expect the area/molecule to increase with decreasing temperature or decrease less than the usual thermal expansion effect. This is, in fact, observed in the hexagonal phase of EP, as discussed below.

In Figure 8, we plot the composite results for the samples as a function of ϕ. In Figure 8a we plot the peak positions of the two orthorhombic peaks as a function of ϕ, at, interpolated to, or extrapolated to, a common temperature of 0 °C. We also include the peak positions for the ethylene−butene copolymers where the much smaller peak shift is clear. The smaller peak shift for the butene copolymers relative to the propylene copolymers suggests lower incorporation or possibly exclusion of the butene units from the crystallites, as was demonstrated by the NMR data discussed earlier. The ratio of the integrated intensities of the two peaks is plotted in Figure 8b. The ratio I_2/I_1 is the ratio of the intensity of the higher-q peak, at q_2, to that of the low-q peak at q_1. Since the low-q peak in the powder pattern has twice the degeneracy of the higher-q peak, the ratio is always <1 and is lower than 0.5 due to form factor effects. The value of $I_2/I_1 \sim 0.25$ is typical for the orthorhombic polyethylene structure. There is a clear segregation of the values for I_2/I_1, which is $\sim$0.25 for $\phi < 0.07$ and much lower for $\phi > 0.09$. In fact, in one sample (EP20-2; $\phi = 0.1021$) only a single peak is observed, and thus $I_2/I_1 = 0$. We will attribute the decrease in the ratio to coexistence of the two-peak orthorhombic phase and the single-peak hexagonal phase, where the first orthorhombic peak is nearly coincident with the hexagonal peak. One can also make the crude approximation that the fraction of crystalline material in the hexagonal phase is $1-4\cdot I_2/I_1$, so for $I_2/I_1 = 0.08$ one would have 68% hexagonal.

In Figure 8c we plot the inverse width, or the correlation length, ξ, associated with the two peaks. The lower-q peak is sharper (larger ξ) for HDPE and low-ϕ materials. The high-q peak appears to broaden continuously from the lowest to the highest ϕ; i.e., ξ_2 decreases continuously. However, as was observed for the intensity ratio I_2/I_1, ξ_1 drops significantly for $\phi > 0.09$ and has values below ξ_2. This extra apparent width is consistent with the observed q_1 peak for $\phi > 0.09$ being a superposition of the single peak corresponding to the hexagonal phase and the first peak corresponding to the orthorhombic phase. These peaks would be close in q, and any difference would add to a slightly increased apparent peak width.

In Figure 8d we show the area per chain which is computed as $A_{\mathrm{ortho}} = 4\pi^2/(q_2\sqrt{{q_1}^2-{q_2}^2/4})$ for the orthorhombic phase. For the high ϕ samples we also compute the area assuming that the q_1 peak position is indicative of the single peak hexagonal phase with $A_{\mathrm{hex}} = 8\pi^2/(\sqrt{3}q^2)$. We see that the lattice expansion in the orthorhombic phase can be fit to $A = 18.41 + 17.30\phi$. Thus, for example, putting a methyl on 5% of the backbone carbons would expand the lattice by $\sim$5%. Trivial packing estimates might thus suggest that all the methyls are included in the lattice. However, since the volume of the CH_3- will be larger than a $-CH_2-$ and since, more importantly, any incorporation of methyl groups into the orthorhombic lattice will cause strain and voids, it is clear that some partitioning of the methyl groups in favor of the amorphous phase regions is consistent with these data. Nevertheless, the incorporation of methyl groups into the orthorhombic lattice is substantial, which is consistent with the SSNMR data discussed earlier.

The hexagonal phase (of which the $\phi = 0.1021$ sample (EP20-2) is pure hexagonal) has an area/molecule of 21 Å^2, which is $\sim$14% greater than that of the HDPE orthorhombic phase. Here, clearly the increased area is due to a decrease in density of packing caused by the disorder and not merely a dense packing of the branched chains. This is similarly observed in the rotator phase of n-alkanes where the area/molecule increases by $\sim$6% on transforming thermotropically from the orthorhombic crystal phase to the rotator phase.[31] We attribute the

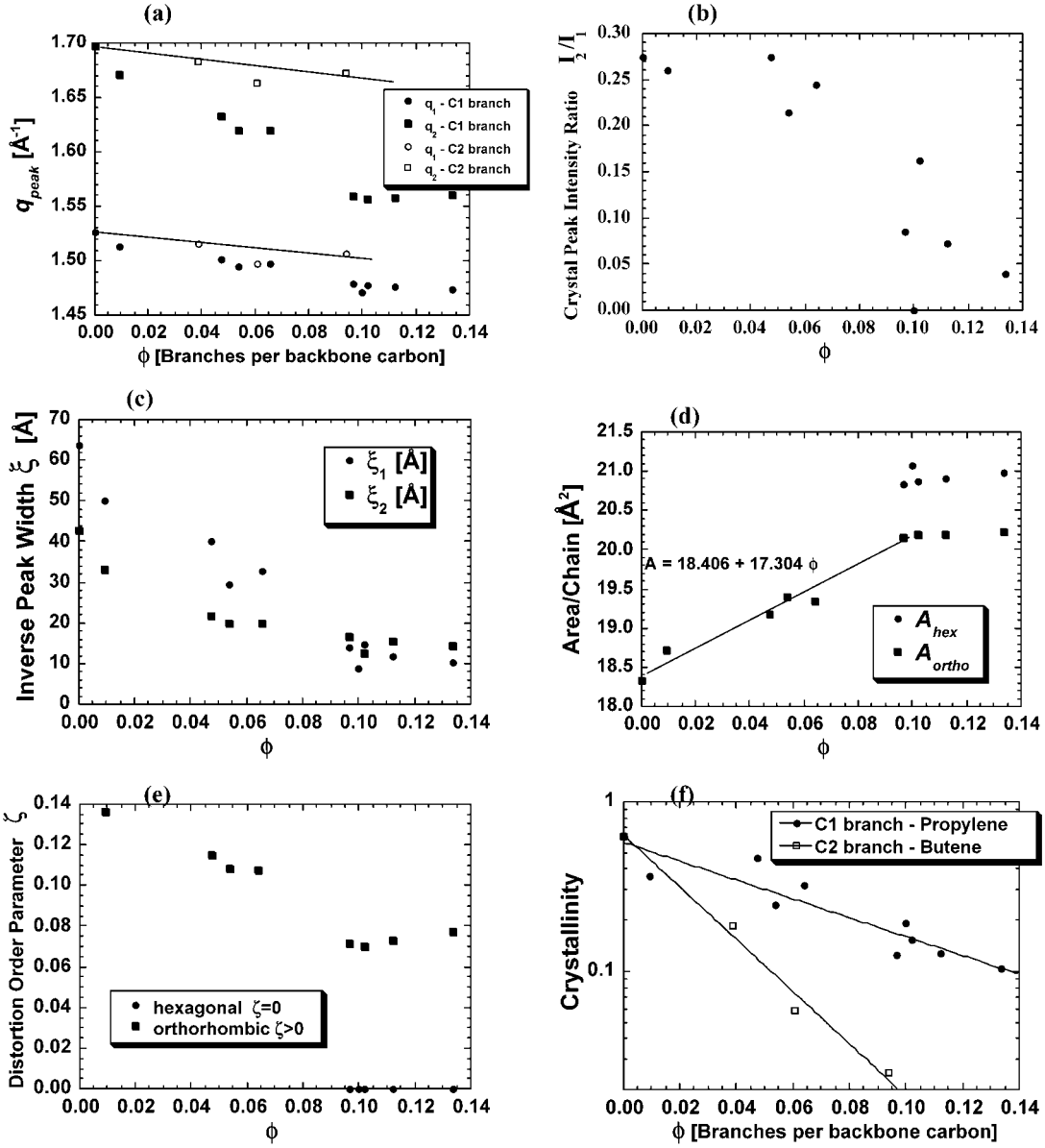

Figure 8. Parameters extracted from scattering scans extrapolated/interpolated to 0 °C as a function of ϕ. (a) The peak positions of the two crystalline peaks, q_1 and q_2. The peak positions for the ethylene−butene copolymers are also included using open symbols. (b) The ratio of the integrated intensities of the two crystalline peaks I_2/I_1. (c) The inverse Lorentzian peak width or correlation length ξ_1 and ξ_2 for the two crystal peaks. (d) The computed area/chain assuming the two peak orthorhombic structure (A_{ortho}) and assuming a single peak hexagonal phase (A_{hex}). (e) The distortion order parameter as described in the text. (f) The crystallinity extracted from the wide angle scattering, for both the propylene and butene copolymers. Included are fits to a simple empirical form $C_{C1} = 0.5748 \exp(-12.789\phi)$ and $C_{C2} = 0.6375 \exp(-35.423\phi)$.

observed 4% increase in the measured areas, A_{ortho} (20.2 Å^2) to A_{hex} (~21 Å^2), to the excess area due to the rotational/conformational disorder. The remaining 10% increase in area from 18.4 to 20.2 Å^2 is due to the incorporation of methyl branches and excess voids created in the orthorhombic crystal. The observed area/molecule of 21 Å^2 resulted from the balance between expanding forces (methyl inclusion, excess voids, and motional freedom) and contracting forces (van der Waals interaction between neighboring CH_2 segments).

Since transitions are often observed between the orthorhombic and hexagonal phases, it has been shown to be useful to characterize the structure in terms of a distortion order parameter which is zero in the hexagonal phase and finite in the orthorhombic.[9,22,32] The order parameter ζ can be defined such that $\zeta = (a^2 - b^2)/(a^2 + b^2)$ where a and b are the major and minor axes of an ellipse drawn through the six nearest neighbors. Thus, $\zeta = 0$ is hexagonal and $\zeta \neq 0$ is orthorhombic. The order parameter is shown as a function of ϕ in Figure 8e. It is clear that the distortion does not go continuously to zero with composition. Rather, it exhibits a discontinuous jump between two structures: a weakly distorted orthorhombic phase and a hexagonal phase.

In Figure 8f we show the crystallinity at 0 °C as a function of ϕ. It is clear that the decrease in crystallinity with branch content is much faster for the ethyl branches than for the methyl branches. The data have scatter probably due to the differences in MW, preparation process, and exact details of sample history and annealing; however, a clear trend of decreasing crystallinity with increasing ϕ is evident. The same trend has been shown by NMR and DSC.

In Figure 9a we plot the temperature derivatives of the peak positions $(-dq/dT)$ as a function of ϕ. As is

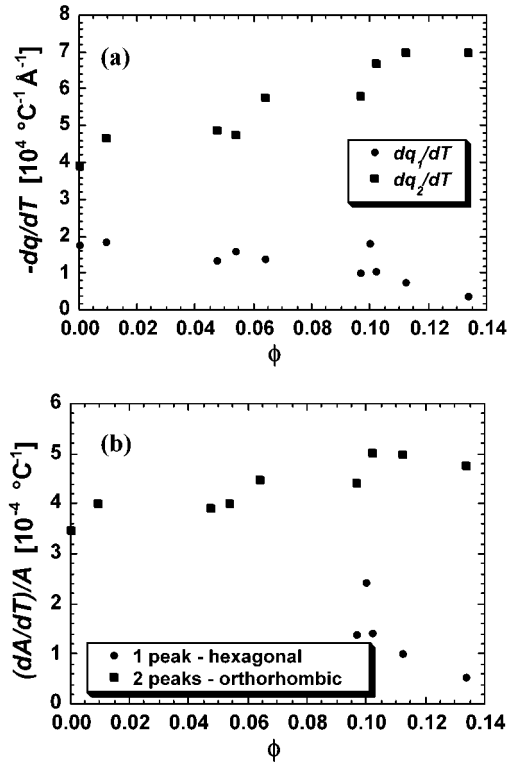

Figure 9. (a) Temperature derivative of the peak positions dq_1/dT and dq_2/dT as a function of ϕ. (b) The 2D thermal expansion derived from the peak position derivatives as a function of ϕ.

apparent from Figure 9a, the change in the high-q peak with temperature is much higher than the corresponding change of the low-q peak. It also shows that the magnitude of dq_2/dT increases with increasing ϕ, while dq_1/dT decreases. In Figure 9b we show the 2D thermal expansion coefficient $(dA/dT)/A$ derived from the peak position derivatives. We compute it both for the orthorhombic phase and the hexagonal phase. We see that the value in the orthorhombic crystal phase is essentially the same as that in the orthorhombic crystal phase of *n*-alkanes, i.e., 5×10^{-4} °C^{-1}.[33] However, in the hexagonal phase the thermal expansion is about an order of magnitude lower than that observed in the hexagonal rotator phase of *n*-alkanes. The low apparent thermal expansion might be caused by an increase in the methyl branch inclusion on decreasing temperature due to increasing crystallinity. As we have observed, the area/chain is strongly dependent on the branch content. Therefore, an increase in the branch content in the crystalline component with decreased temperature would result in a reduction of the apparent thermal expansion.

These combined X-ray results show clearly that, on adding branches, there is an expansion of the lattice and a decrease in the orthorhombic distortion. However, this does not proceed in a structurally continuous way to the hexagonal phase. There is no structure with very small distortion order parameter. This is similar to the behavior of the shorter alkanes and related systems, where the structure transforms to the hexagonal phase through a first-order transition, compositionally as well as thermally.[9,34] Since first-order transitions usually exhibit hysteresis, semicrystalline polymers do not reach their equilibrium states, and the distribution of branches along the polymer chain is statistical rather than uniform, the coexistence of the phases is not surprising.

Table 4. DSC Results of EP and EB Copolymers

sample	first melt (°C)	crystallization temp (°C)	second melt (°C)	heat of melting (J/g)
EB11	42.9, 65.6	48.2	64.2	46
EB16	10.6, 46.2	12.8, 28.8	48.1	16
EP20-2	5.8, 45.3	15.6, 26.9	30.2	31
EP10	~50, 82.1	67.4	79.9	77
EP8	~50, 101.0	56.9, 83.7	100.6	110

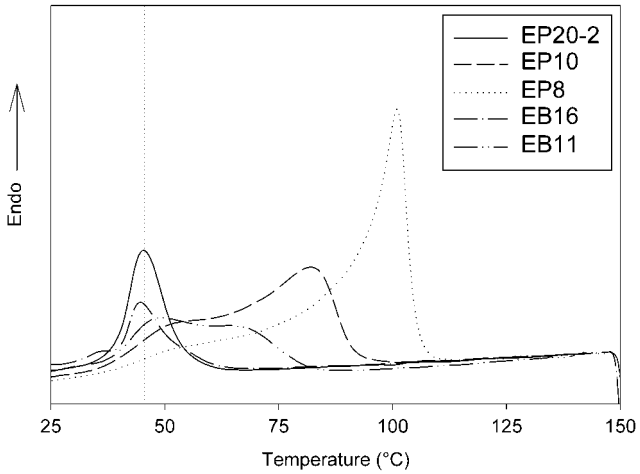

Figure 10. DSC scans of EP and EB copolymers.

Thermal Properties. The crystallization and melting behavior of the copolymers were investigated using differential scanning calorimetry (DSC), and the results are shown in Table 4. The samples were heated in the DSC from −75 to 150 °C at 10 °C/min, held for 2 min, cooled to −75 °C at 10 °C/min, held for 5 min, then reheated to 150 °C at 10 °C/min. The results of these scans are termed as the first melt, crystallization temperature, and second melt, respectively, in Table 4. The heat of melting reported in the table is the area under the first heat melting endotherm.

The first heat DSC scans of some of the EP and EB copolymers are shown in Figure 10. It is interesting to note that all samples displayed broad melting endotherms unlike that typically observed for HDPE. In addition, all samples showed at least two melting endotherms in the first heat. One of the endotherms was always observed at ~45−50 °C (shown by the dotted line in the figure), and the other varied with comonomer content. We attribute the endotherm at ~50 °C to the occurrence of secondary crystallization due to annealing at room temperature. A detailed investigation of the origin and nature of this multiple melting behavior has been reported by Marand et al.[35] and will not be discussed here. Only the area under the endotherm(s) observed above 25 °C are shown in the table, since in the high comonomer containing polymers, lower endotherms are also observed below room temperature but would not contribute to any physical properties at room temperature. Figure 11a shows the first heat and second heat melting temperatures of a series of EP copolymers. Note that there are more samples here than are listed in Table 1. The melting temperature corresponding to the most prominent endotherm has been plotted in this figure. As expected, the melting temperature decreased with increasing propylene content. The second heat melting temperatures for the high propylene containing copolymers are below the first heat; this is due to an increase in the melting temperature with storage time

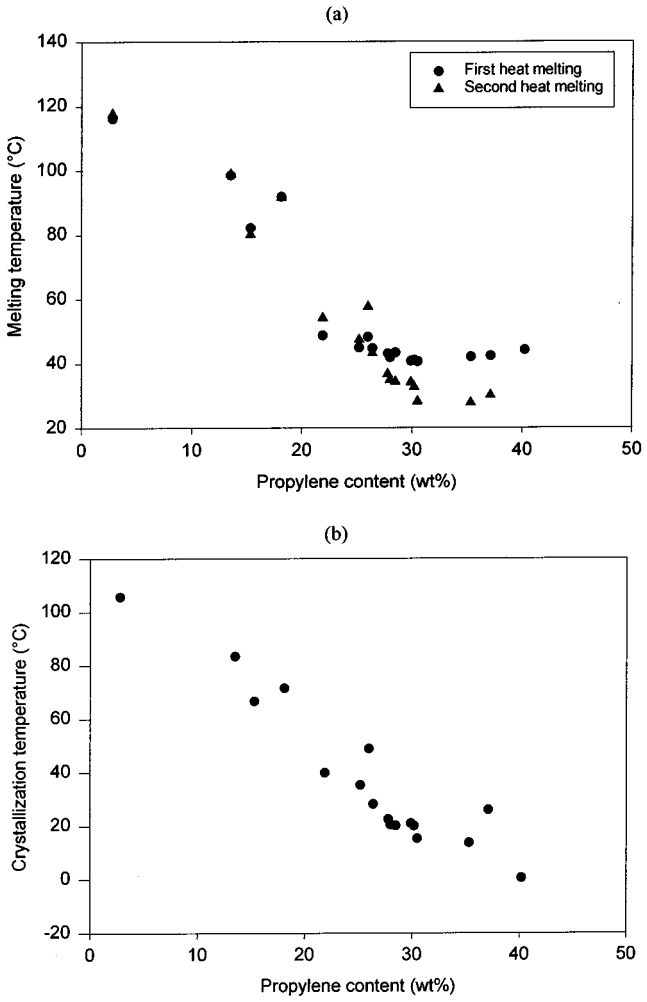

Figure 11. (a) Melting temperature and (b) crystallization temperature of EP copolymers.

at room temperature due to secondary crystallization effects. This annealing at room temperature also causes the observed melting temperature to appear to be independent of comonomer content for propylene content above ~25 wt %. Figure 11b shows the crystallization temperature on cooling of EP copolymers, which shows the crystallization temperature to decrease with increasing propylene content, as would be expected. At the higher comonomer contents, the crystallization temperature is below room temperature. For such samples that are quenched to room temperature, both primary and secondary crystallization would take place at room temperature. It is interesting to note that the melting and crystallization behavior did not show any marked differences between the formation of orthorhombic crystals (low comonomer content), mixed orthorhombic and hexagonal crystals (medium comonomer content), and hexagonal crystals (high comonomer content). The dependence of melting temperature and crystallization temperature on comonomer content does not show any breaks or discontinuities. This is expected since the WAXS results showed that despite the first-order nature of the transition, there is substantial phase coexistence which would smear out any discontinuities in behavior as a function of comonomer content. The dependence of heat of fusion on comonomer content is essentially identical to that observed for the crystallization temperature, with a monotonic decrease observed with increasing propylene content.

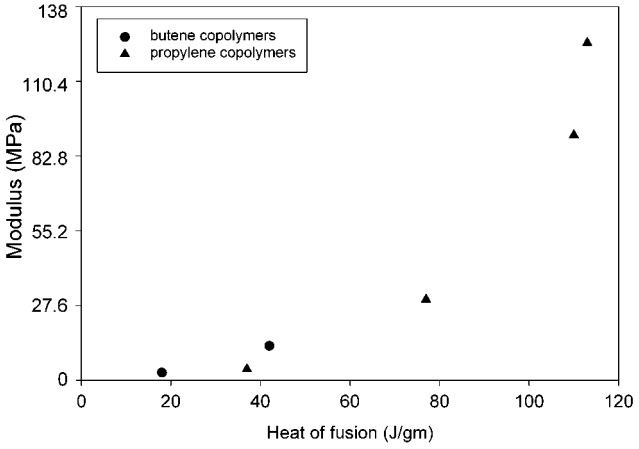

Figure 12. Modulus vs heat of fusion of EP and EB copolymers.

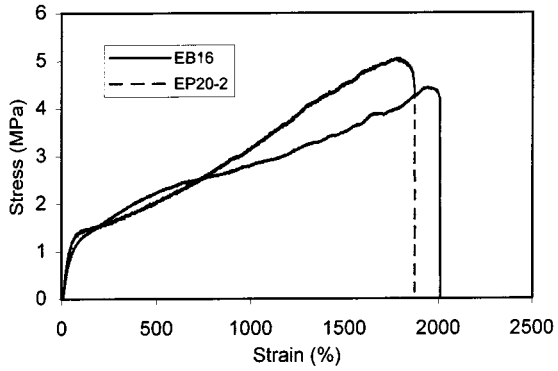

Figure 13. Stress−strain curve comparison of EP and EB copolymers.

Since the NMR results and the WAXS data showed that the EP copolymers crystallized in the hexagonal phase at higher comonomer contents, it is hazardous to compare the degree of crystallinity of the various samples using heat of fusion data. Likewise, it would not be easy to compare the melting temperature data, unless independent information on the crystalline phase of the sample was available. Nevertheless, a comparison of the melting temperature and heat of fusion of the copolymers suggests that EP copolymers display a higher melting temperature and heat of fusion (perhaps degree of crystallinity) than EB copolymers at similar comonomer contents. A comparison of the EP copolymer with ~10 mol % comonomer (EP10) with an EB comonomer with ~11 mol % comonomer (EB11) shows that the EP copolymer has a higher melting temperature and heat of fusion than the EB copolymer. Note that SSNMR and WAXS results showed substantially similar results as well. Comparison of an EP copolymer with ~20 mol % comonomer (EP20-2) with an EB copolymer with ~16 mol % comonomer (EB16) shows that the EP copolymer has a higher heat of fusion compared to that of the EB copolymer. Note that in this case EP20-2 is in the hexagonal form and EB16 has orthorhombic crystals. Overall, the results strongly indicate the formation of larger fractions of crystalline domains in EP copolymers compared to EB copolymers due to the incorporation of propylene sequences in the crystalline regions.

Mechanical Properties. The mechanical properties of the EP and EB copolymers are shown in Table 5 and Figures 12 and 13. Inspection of Table 5 shows that the modulus of the polymers essentially follow the same

Table 5. Mechanical Properties of EP and EB Copolymers

sample	modulus (psi)	break strain (%)	permanent set (%)
EB11	1836	1130	38
EB16	411	1934	12
EP20-2	595	1794	10
EP10	4325	1077	98
EP8	13120	1359	143

trends as the heat of fusion, as is also shown in Figure 12. The modulus is a measure of the low-strain properties of a material and is typically a strong function of the degree of crystallinity of the material. Note that in this series are samples that exhibit the hexagonal crystals and some samples that exhibit orthorhombic crystals, as shown by SSNMR and WAXS data discussed earlier. There seems to be no differentiation of these two types in the trend observed in Figure 12.

The permanent set values were larger for the higher modulus polymers, indicating permanent deformation was larger for the larger crystallinity polymers. Again, from this limited data set, there appears to be no dependence of permanent set on comonomer type. The strain at break also did not show any dependence on comonomer type or content, though there was a definite dependence on molecular weight, with the higher molecular weight samples displaying a lower strain at break. Such behavior has been previously observed for polyethylene copolymers and attributed to the role of increased entanglements in the higher molecular weight polymers.[36,37]

Figure 13 shows the stress−strain plots of an EP copolymer which displays the rotator phase (EP20-2) and an EB copolymer which displays the orthorhombic phase (EB16). Because of a higher degree of crystallinity, the EP copolymer shows a yield behavior at low strains, followed by strain hardening behavior until the break point. In contrast, the EB copolymer does not display a well-defined yield (though a weak yield region is evident) and also shows strain hardening until break. Given the fact that these samples display different crystal forms, there seems to be little qualitative difference between the stress−strain curves that can be attributed to the nature of the crystal phase. This may be because both kinds of crystallites exhibit fast chain dynamics, even though the modes of motion are different. The crystalline domains in these samples likely act as junction points, while the deformation is governed by the large amorphous fraction.

Discussion

Effect of Methyl Branch Inclusion in Crystallites on Isotropic Chemical Shift. The change of lattice constants on increasing propylene content corresponds to a downfield change in isotropic chemical shift of the orthorhombic crystalline signal. As seen in Figure 2, from a propylene content of 0−13 mol %, the ICS increases by 0.3 ppm (from 32.8 to 33.1 ppm). The change of crystalline ICS with comonomer content is much smaller for EB copolymers: ICS increases from 32.8 to 32.9 ppm for the comonomer content range of 0−16 mol %. Such a difference of crystalline ICS between EP and EB copolymers again shows the effect of methyl branch incorporation.

The question naturally following the above observation is: what is the mechanism of such a change in ICS? To answer the question, it may help to recall the fact that the monoclinic and orthorhombic phases in high-density polyethylene exhibit significantly different chemical shift values (34.2 vs 32.8 ppm), even though the two phases have very similar packing density. This suggests that packing density is not the governing factor for the differences in isotropic chemical shift. Rather, the relative orientation of neighboring chains—the planes of neighboring chains being perpendicular (orthorhombic), parallel (monoclinic), or an average between perpendicular and parallel (rotator)—seems more important: ICS (perpendicular) = 32.8 ppm, ICS (parallel) = 34.2 ppm, while ICS of rotator phase is approximately midway between the two extremes (33.4 ppm). Extending this postulation to methyl-branch-containing orthorhombic crystallites, a feasible explanation is that methyl inclusion introduces more libration mode to the chain motion, which averages the relative orientation between neighboring chains and causes the change in ICS. This is supported by the pattern of lattice change (*a* increases while *b* is constant) upon increasing methyl branch content, which should accommodate more axially symmetric motional modes (also see next section).

Structural and Dynamic Characteristics of the Rotator Phase. In the rotator phase in EP copolymers, each chain has approximate rotational symmetry. In addition, the rotation of neighboring chains is probably not correlated (or weakly correlated), due to bulkiness of the methyl branches. Packing of these axially symmetric chains is naturally hexagonal. Therefore, the rotator phase observed by NMR should be the hexagonal phase detected by X-ray scattering. It has been proposed that the hexagonal phase in EP copolymers is a "pseudohexagonal" phase—it has the orthorhombic unit cell with lattice constants that happen to have hexagonal symmetry.[3] In light of the different molecular dynamics in orthorhombic and rotator crystallites discussed above, we feel that this concept needs to be revisited. In the following, we will discuss several observations that made us believe that the rotator/hexagonal phase is distinguished from the orthorhombic phase by a matter of symmetry.

First, X-ray data suggest that as propylene content increases, the crystalline lattice does not seem to enter the hexagonal phase in a continuous way. Even in the samples where the two phases coexist, the lattice constants of the two phases are remarkably different. Considering the narrow composition distribution nature of the samples, this suggests that there is likely an abrupt transition from orthorhombic to hexagonal phase as propylene content increases.

Second, the lattice constants and area per chain of the orthorhombic phase continuously change with composition, while those of the rotator phase do not noticeably change. Similarly, the isotropic NMR chemical shift of the rotator phase, which is determined by lattice constants and molecular dynamics, also stays at ∼33.4 ppm for propylene content of 20−27 mol %. These again support the view that the rotator phase is not just an orthorhombic lattice with coincidental lattice constants, but rather a different state.

Finally, the $S_{\alpha\delta+}$ resonance in the orthorhombic phase is broad and not resolved from the amorphous counterpart, while that in the rotator phase is relatively narrow and well resolved. This suggests that the branch point in the rotator phase has a well-defined trans conformation as a result of the chain rotation. In other words, there is little static disorder in the neighborhood of branching point. On the other hand, since the flip

motion in the orthorhombic phase is less intense than continuous rotation, the branch point cannot be completely straightened and is thus more "kink"-like (though still nearly trans, as its ICS is in between rotator and amorphous $S_{\alpha\delta+}$ signals)—possessing a broader distribution of conformation. Therefore, the difference in the signal width and splitting supports the notion that the motional modes in the two phases are different.

Combining the observations from solid-state NMR and X-ray scattering, we propose the following hypothetical picture that may help to understand why (1) lattice constant *a* increases much more than *b* upon increasing propylene content and (2) rotator (or hexagonal) phase is a distinct state and the natural destination of the orthorhombic lattice expansion. In the ethylene crystallites that do not contain methyl branches, the motion of the chains is a 180° flip. The flip motion is not axially symmetric with respect to the chain axis, reflecting the constraint from the orthorhombic lattice. In the crystallites that contain methyl branches, flip becomes less favorable than rotation because the local segments containing the branch do not have a flip-and-slip symmetry as does an all-trans ethylene chain. As a result, a certain amount of rotation (i.e., libration) is added to the motional mode. Since this component gives chains more cylindrical symmetry, it causes the lattice change from orthorhombic toward hexagonal. In other words, the fact that the lattice constant *a* changes much more than *b* is because the lattice needs to accommodate more and more axially symmetric motional mode. With increasing branch content, more and more libration is added to the flip motion, and eventually chain rotation is introduced. Such a picture seems to be able to explain the essential observations in this report, and it may be experimentally verified using appropriately designed techniques.

Conclusions

The morphology and physical properties of a series of ethylene−propylene and ethylene−butene copolymers were studied using solid-state NMR, WAXS, DSC, and mechanical measurements. On increasing propylene content, the orthorhombic "PE" unit cell expands anisotropically and becomes less distorted with respect to hexagonal, undergoing a compositionally driven first-order transition to the rotator/hexagonal phase at higher propylene contents. The structure therefore does not go continuously from finite ζ to $\zeta = 0$ (hexagonal). The isotropic chemical shift, powder pattern, and ^{13}C T_1 relaxation time show that the crystallites in EP copolymers are rotator/hexagonal when the propylene content is high (>20 mol %), which is a result of the incorporation of methyl branches in the crystallites. It is proposed that the transition into the rotator/hexagonal phase is closely related to the change of molecular dynamics upon increasing methyl branch content. Ethyl branches are difficult to incorporate in the crystallites, so the crystallites in EB copolymers remain in the orthorhombic form. At a given comonomer mole percentage, EB copolymers have lower crystallinity and modulus than EP copolymers. The mechanical properties of EP and EB copolymers do not appear very different in the window of the comonomer content of interest. However, the detailed dependence of mechanical properties on comonomer type is not clear in this study due to the limited samples available for investigation.

Acknowledgment. The authors thank Prof. K. Schmidt-Rohr for helpful discussion and Steve Bennett for technical assistance. Part of this research was carried out at the National Synchrotron Light Source, Brookhaven National Laboratory, which is supported by the U.S. Department of Energy, Division of Materials Sciences and Division of Chemical Sciences, under Contract DE-AC02-98CH10886.

References and Notes

(1) Bassi, I. W.; Corradini, P.; Fagherazzi, G.; Valvassori, A. *Eur. Polym. J.* **1970**, *6*, 709.
(2) Shirayama, K.; Kita, S.; Watabe, H. *Makromol. Chem.* **1972**, *151*, 97.
(3) Baldwin, F. P.; Ver Strate, G. *Rubber Chem. Technol.* **1972**, *45*, 709.
(4) Howard, P. R.; Crist, B. *J. Polym. Sci., Polym. Phys. Ed.* **1989**, *27*, 2269.
(5) de Ballesteros, O. R.; Auriemma, F.; Guerra, G.; Corradini, P. *Macromolecules* **1996**, *29*, 7141.
(6) Guerra, G.; de Ballesteros, O. R.; Venditto, V.; Galimberti, M.; Sartori, F.; Pucciariello, R. *J. Polym. Sci., Polym. Phys. Ed.* **1999**, *37*, 1095.
(7) Wright, K. J.; Lesser, A. J. *Macromolecules* **2001**, *34*, 3626.
(8) Androsch, R.; Blackwell, J.; Chvalun, S. N.; Wunderlich, B. *Macromolecules* **1999**, *32*, 3735.
(9) Sirota, E. B. *Langmuir* **1997**, *13*, 3849.
(10) Ungar, G. *Macromolecules* **1986**, *19*, 1317.
(11) Kuwabara, K.; Horii, F. *Macromolecules* **1999**, *32*, 5600.
(12) Sirota, E. B.; Herhold, A. B. *Science* **1999**, *283*, 529.
(13) Kraack, H.; Deutsch, M.; Sirota, E. B. *Macromolecules* **2000**, *33*, 6174.
(14) Keller, A.; Cheng, S. Z. D. *Polymer* **1998**, *39*, 4461.
(15) Perez, E.; VanderHart, D. L. *J. Polym. Sci., Polym. Phys. Ed.* **1987**, *25*, 1637.
(16) Hosoda, S.; Nomura, H.; Gotoh, Y.; Kihara, H. *Polymer* **1990**, *31*, 1999.
(17) Perez, E.; VanderHart, D. L.; Crist, B.; Howard, P. R. *Macromolecules* **1987**, *20*, 78.
(18) Torchia, D. A. *J. Magn. Reson.* **1978**, *30*, 613.
(19) Wang, Z. G.; Hsiao, B. S.; Sirota, E. B.; Agarwal, P.; Srinivas, S. *Macromolecules* **2000**, *33*, 978.
(20) Hu, W.-G.; Schmidt-Rohr, K. *Polymer* **2000**, *41*, 2979.
(21) Ishikawa, S.; Kurosu, H.; Ando, I. *J. Mol. Struct.* **1991**, *248*, 361.
(22) Sirota, E. B.; H. E. King, J.; Singer, D. M.; Shao, H. H. *J. Chem. Phys.* **1993**, *98*, 5809.
(23) Ishikawa, S.; Ando, I. *J. Mol. Struct.* **1993**, *291*, 183.
(24) VanderHart, D. L. *J. Magn. Reson.* **1981**, *44*, 117.
(25) VanderHart, D. L. *J. Magn. Reson.* **1987**, *72*, 13.
(26) Opella, S. J.; Waugh, J. S. *J. Chem. Phys.* **1977**, *66*, 4919.
(27) Hu, W.-G.; Boeffel, C.; Schmidt-Rohr, K. *Macromolecules* **1999**, *32*, 1611.
(28) Hu, W.; Schmidt-Rohr, K. Unpublished results.
(29) Carman, C. J.; Harrington, R. A.; Wilkes, C. E. *Macromolecules* **1977**, *10*, 536.
(30) Axelson, D. E.; Mandelkern, L.; Popli, R.; Mathieu, P. *J. Polym. Sci., Polym. Phys. Ed.* **1983**, *21*, 2319.
(31) Small, D. M. *The Physical Chemistry of Lipids*; Plenum: New York, 1986.
(32) Kaganer, V. M.; Peterson, I. R.; Kenn, R. M.; Shih, M. C.; Durbin, M.; Dutta, P. *J. Chem. Phys.* **1995**, *102*, 9412.
(33) Sirota, E. B.; Singer, D. M.; H. E. King, J. *J. Chem. Phys.* **1994**, *100*, 1542.
(34) Sirota, E. B.; H. E. King, J.; Shao, H. H.; Singer, D. M. *J. Phys. Chem.* **1995**, *99*, 798.
(35) Alizadeh, A.; Richardson, L.; Xu, J.; McCartney, S.; Marand, H.; Cheung, Y. W.; Chum, S. *Macromolecules* **1999**, *32*, 6221.
(36) Kennedy, M. A.; Peacock, A. J.; Mandelkern, L. *Macromolecules* **1994**, *27*, 5297.
(37) Popli, R.; Mandelkern, L. *J. Polym. Sci., Part B: Polym. Phys. Ed.* **1987**, *25*, 441.

MA0118670